COMPOSITE DESIGN EXPERIENCE USING MSC NASTRAN FOR THE HYDRODYNAMIC FAIRINGS OF A NEW SUBMERSIBLE

Dr. E. Thomas Moyer Jr., Dr. Richard Cobb, Mr. Kim Grubbs
Analysis and Technology Inc., Engineering Technologies Group
and
Dr. William Gordon
Northrop-Grumman Corporation, Oceanic Systems

This paper details our recent experiences designing the fairings for a new submersible vehicle being constructed. A unique composite material design approach was chosen to meet challenging structural requirements while minimizing weight. Analysis examples include material selection decisions, laminate design tradeoff studies, modeling of bolted joints, establishment of material allowables and global/local analysis approaches.

1] Introduction

Analysis & Technology, Inc./Engineering Technologies Group (A&T/ETG) was tasked to design hydrodynamic fairings for a new submersible vehicle. The outer molded geometry of the fairings was determined due to the hydrodynamic requirements of the craft. This provided a design surface which defined the outer shape. Figure 1 shows a schematic of the craft.

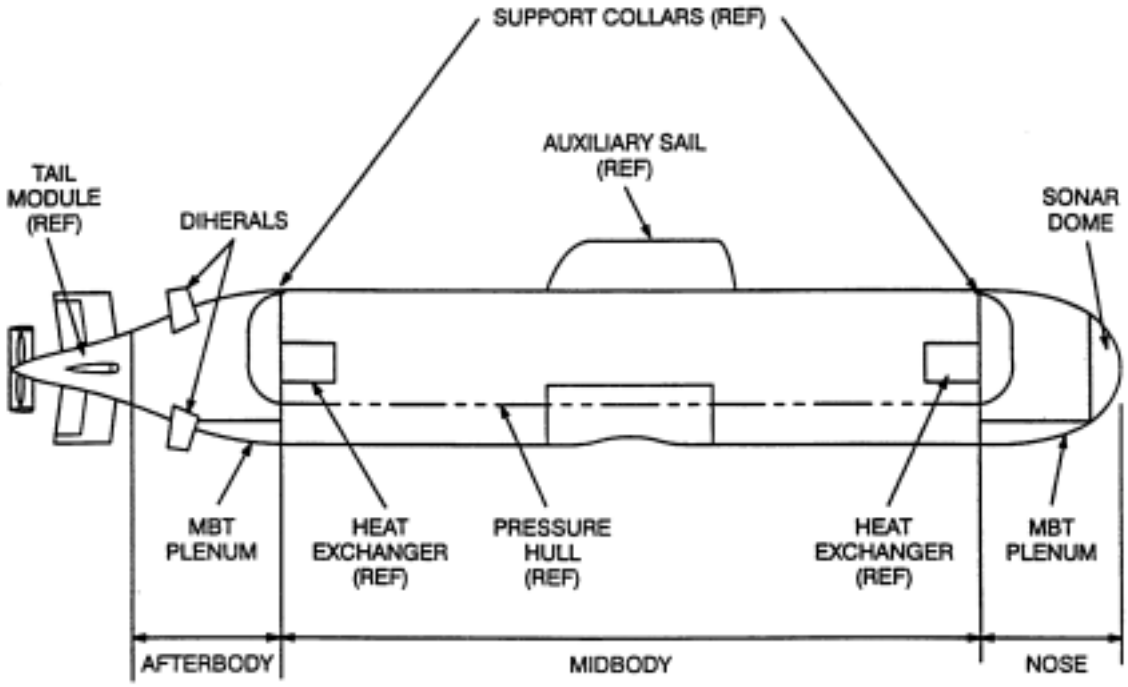

Figure 1: Geometry of the Submersible

The fairings are divided into three distinct sections: the nose fairing, the midbody fairing panels and the aft fairing, each with independent requirements. The nose connects to the pressure hull of the craft at eight lugs welded to the steel collar. The sonar dome is connected to the front end of the nose fairing. The aft fairing connects to a similar steel collar at the aft end of the pressure hull (also through eight lugs). The tail section bolts to the aft end of the aft fairing. Surrounding the pressure hull are the midbody fairing panels. The midbody panels consist of discrete fairing panels which must be easily removable to provide access to equipment/systems foundationed to the hull. Due to space limitations, this paper will discuss the design of the nose/aft fairings and its connection to the pressure hull support collar. MSC NASTRAN [1] was the primary analysis tool used in the design process. Both linear and elastic-plastic analyses were performed. All analyses were performed under Windows NT using a 300 MHz Pentium II processor, 128Mb of RAM and a 10 Gb SCSI hard disk drive.

2] Nose/Aft Design Requirements

The nose/aft fairings are separate structural systems which share many design features and requirements. Various loading conditions are defined to reflect both operational loads and extreme loads anticipated in use. The controlling load cases to be discussed in this paper include an operational load case where 1000 psf pressure is applied to the top of the structure while subjected to a 1 g inertial load. Inertial loads include 30% of the entrained and entrapped water of the flooded fairing structure. It was determined that this was the effective “added mass” acting on the structure while submerged. The second load case considered in this paper is an extreme load case (anticipated to occur very infrequently). This load is a 20 g inertial load in any direction.

Due to weight considerations it was decided to use a rubber toughened epoxy/glass prepreg composite for the outer surface of the nose/aft fairings. This material has excellent fracture toughness properties in addition to good stiffness, strength and damage tolerance. The good fracture toughness provides the structure with good impact resistance. It was envisioned early on that the nose/aft structures would be skin stiffened shells. The structural configuration is presented in detail in the next section. Internal structure (for stiffeners, internal bulkheads, etc.) could be constructed from any readily available composite materials. Both prepreg carbon/epoxy and Vacuum Assisted Resin Transfer Molded E-glass/Vinylester (VARTM glass) composites were employed. Metallic parts were to be made from ELI grade titanium for weight/strength/corrosion considerations.

To assess structural integrity, it was decided to use a component by component failure approach. For laminate composites the stress in the warp,

fill and in-plane shear direction for each lamina were compared with lamina allowables for those components. For operational load cases, a factor of safety of four (4) was imposed on all lamina strengths. This large factor provides good fatigue life and some margin due to ignoring combined failure mode effects. For the extreme load case, no safety factor is employed. The requirement for the extreme load is that the overall integrity of the structure must be maintained, however, local damage is permitted. Under extreme loading, slight local stress excesses were, therefore, tolerated. For operational load cases, a factor of safety of 2 on yield was employed for metals. For the extreme load case, ultimate strength (compared to principal stresses) was used. A detailed elastic-plastic analysis was employed for the attachment to the pressure hull.

3] Nose/Aft Model Features

Figure 2 provides a picture of the global finite element model of the nose fairing.

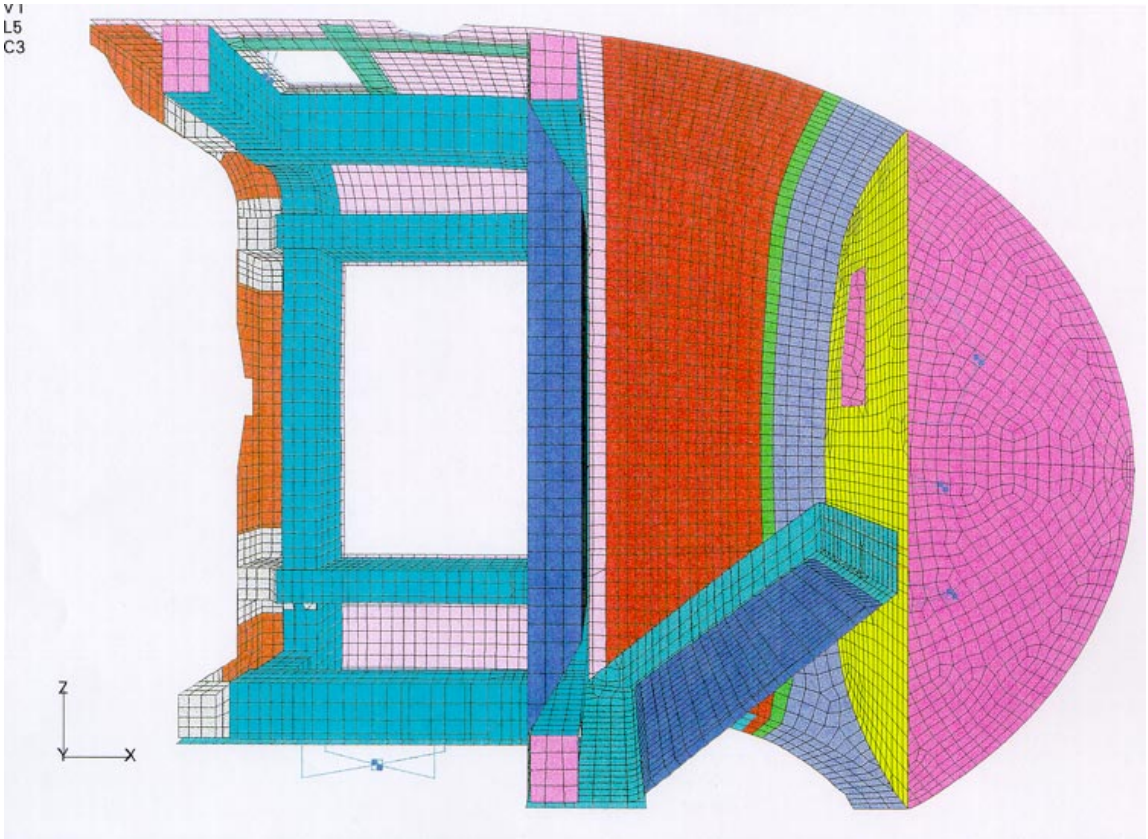

Figure 2: Nose NASTRAN Model

This model assumes symmetry about the longitudinal center plane of the vehicle. The colors refer to the NASTRAN properties of the model. Basically,

the structure is a stiffened shell structure with on internal bulkhead. The major opening in the side of the fairing is for the vehicle thrusters and is covered by thruster doors. The shell is stiffened by C channels constructed from prepreg carbon/epoxy composites. The stiffeners are bolted to the shell with titanium bolts. The full model is comprised of approximately 28,000 nodes and 32,000 elements.

All composite laminates in the submersible Nose Fairing structure are modeled using layered shell elements (CQUAD4 and CTRIA3 elements). These include the E-Glass outer skin, floor, and forward bulkhead; the carbon L-channel, longerons, transverses, and roof bracing; and the VARTM GRP vertical and sloped bulkheads. Individual ply thicknesses, material sets, and angular orientations for each particular lamina are fully detailed in the element descriptions. Laminate properties are specified using the PCOMP property card with MAT8 material properties. The 1" thick and 6" thick syntactic foam cores (for the sloped bulkhead and the vertical bulkhead, respective), are modeled using solid elements. The sonar dome on the submersible Nose is also modeled with layered shell elements, using element descriptions and material properties provided for the system. The sonar dome will not be discussed in detail in this paper.

All of the composite structural elements in the submersible Nose Fairing are joined using titanium bathtub fittings. The entire nose structure is then connected to the submersible forward support collar through the use of eight titanium clevi. These titanium pieces are represented in the submersible Nose models as discrete components, modeled using isotropic plate elements. The bolts connecting the various structural components of the submersible Nose are discretely modeled as stiff bar elements. The bar elements are not permitted to transmit torsion, however, they can transmit axial force, two components of shear force and two bending moments.

Equipments which are foundationed to the submersible Nose Fairing structure are modeled using point masses connected to the fairing structure with stiff bar elements. All equipments weighing over 15 lb. are included in the models.

4] Material Systems

The nose/aft fairings employ three composite material systems, the rubber toughened epoxy GRP prepreg (E-Glass), the carbon/epoxy prepreg and the VARTM GRP. Since the vessel operates in seawater, strength degradation due to moisture absorption must be considered. For the purposes of design, the stiffness data used are "dry" values. All properties are computed as "B-Basis" values. Dry moduli are typically higher than "wet" moduli. Using dry stiffness properties, therefore, tends to predict conservative stresses. Strength

properties were wet values. Wet properties are produced by submersing the test specimens in 95 degree C synthetic seawater for 72 hours. The samples are then tested (as soon as practicable) using the standard test methods. Table 1 provides a summary of the material properties used in the design. All properties were generated by testing samples made by the fairing fabricator using production fabrication processes. Tests were conducted by Penn State Universities Applied Research Laboratory.

Table 1. Material Properties and Strengths

Stress State	E-Glass	Carbon cloth	VARTM GRP
E-Warp	3.0 msi	10.5 msi	3.3 msi
E-Fill	2.7 msi	9.7 msi	3.0 msi
E-Transverse	1.4 msi	-	-
G-In Plane	550 ksi	850 ksi	660 ksi
G-Transverse	430 ksi	850 ksi	572 ksi
Poisson In Plane	0.15	0.15	0.15
Warp Strength	39.1 ksi	75.0 ksi	41.4 ksi
Fill Strength	33.7 ksi	61.0 ksi	37.1 ksi
Bearing Strength	48.3 ksi	95.4 ksi	48.3 ksi
Transverse Tensile Strength	5.54 ksi	-	-
Interlaminar Shear Strength	5.53 ksi	-	-
In-Plane Shear	9.41 ksi	7.5 ksi	12.5 ksi
Weight Density (lbs/in ^{3})	0.0680	0.0560	0..0680

4] Stress Results Nose/Aft

Figure 3 shows a plot of the warp stress in the nose outer shell (skin) for ply 25.

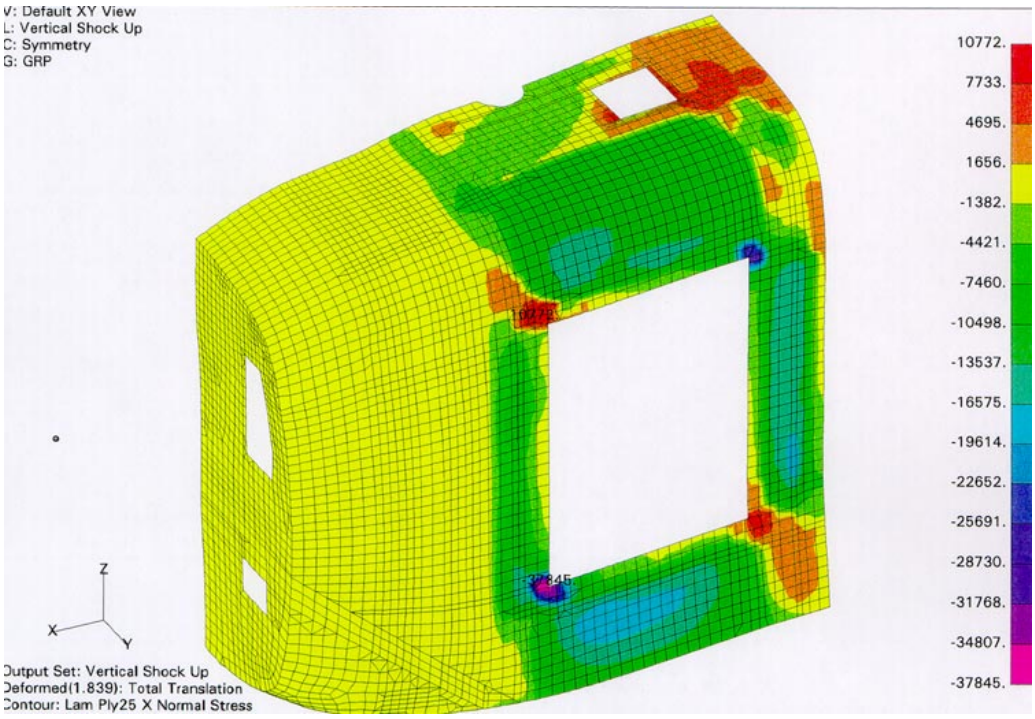

Figure 3: Warp Stress Distribution In Nose Shell

The layup of the shell is quasi-isotropic. The outermost and innermost plies of unique orientation (0/45/90/-45 plies) are examined stress component by stress component. All stresses are reported in the material coordinate system which specified X as the warp direction and Y as the fill direction. This stress plot is for the extreme load case of 20 G inertial loading in the positive Z direction (global direction). In the corners of the opening for the thruster door, large stress concentrations are predicted. This is due to the loads from the thrusters which tend to rack the opening combined with the modeling as a sharp corner. In reality, the corners will have a radius which can be analyzed with a local model. In addition to the thruster door corners, stress concentrations are observed in the roof due to the required cutouts.

Figure 4 shows the stress distribution in the carbon channels highlighting the regions of highest stress.

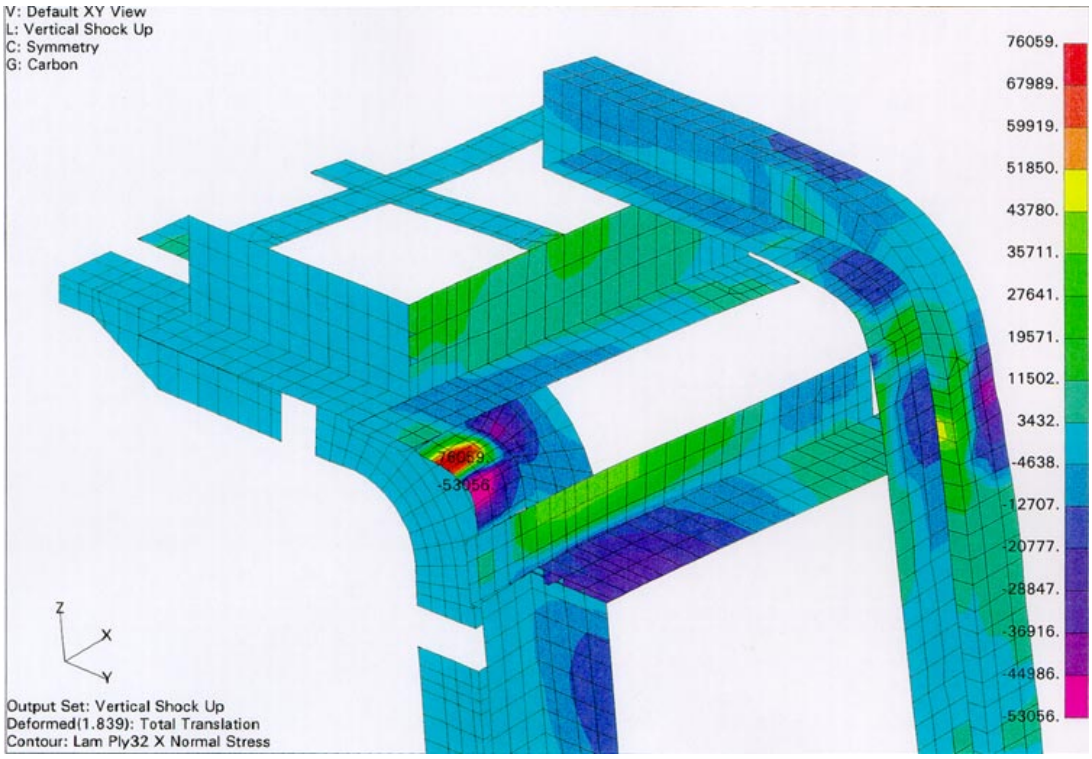

Figure 4: Stress Distribution In Carbon Channels

A large concentration is observed in the radius of the channel transferring load from the roof to the side structure. Other (smaller) stress concentrations are observed where the discrete bolts attach to the channels. This stress component is a warp stress in one of the outermost carbon lamina.

Figure 5 shows the stress distribution in the vertical sandwich bulkhead which is made of the VARTM glass material.

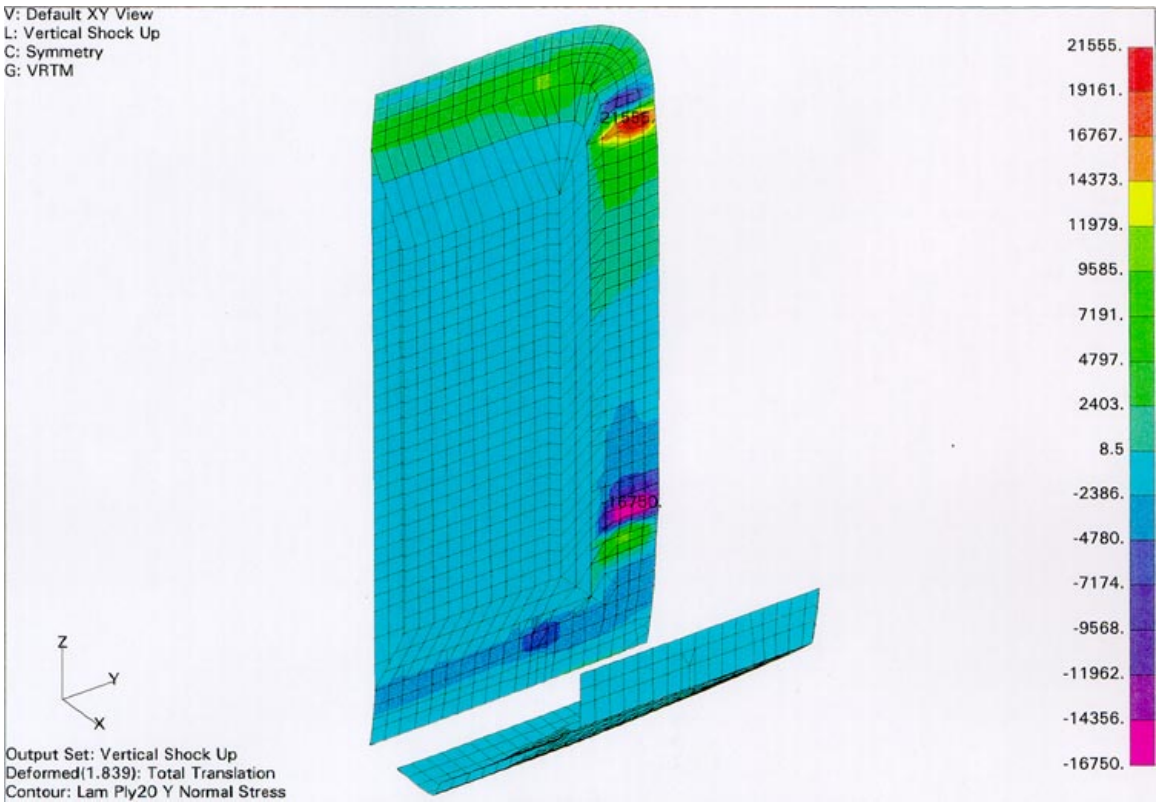

Figure 5: Warp Stress In VARTM Bulkhead

The warp stress in an outer ply is shown. The core of the sandwich is 24 pcf foam (which was modeled with solid elements). Stress concentrations are observed near the two side joint regions where the channels bolt to the bulkhead. Titanium inserts are used to stiffen all intersections of the carbon channels with other structure (e.g. corners where carbon stiffeners meet and where the carbon stiffeners connect to and frame the bulkhead.

Figure 6 shows a typical shear stress distribution in the shell for the case where 1000 psf pressure is applied to the top of the structure while subjected to a 1 g inertial load.

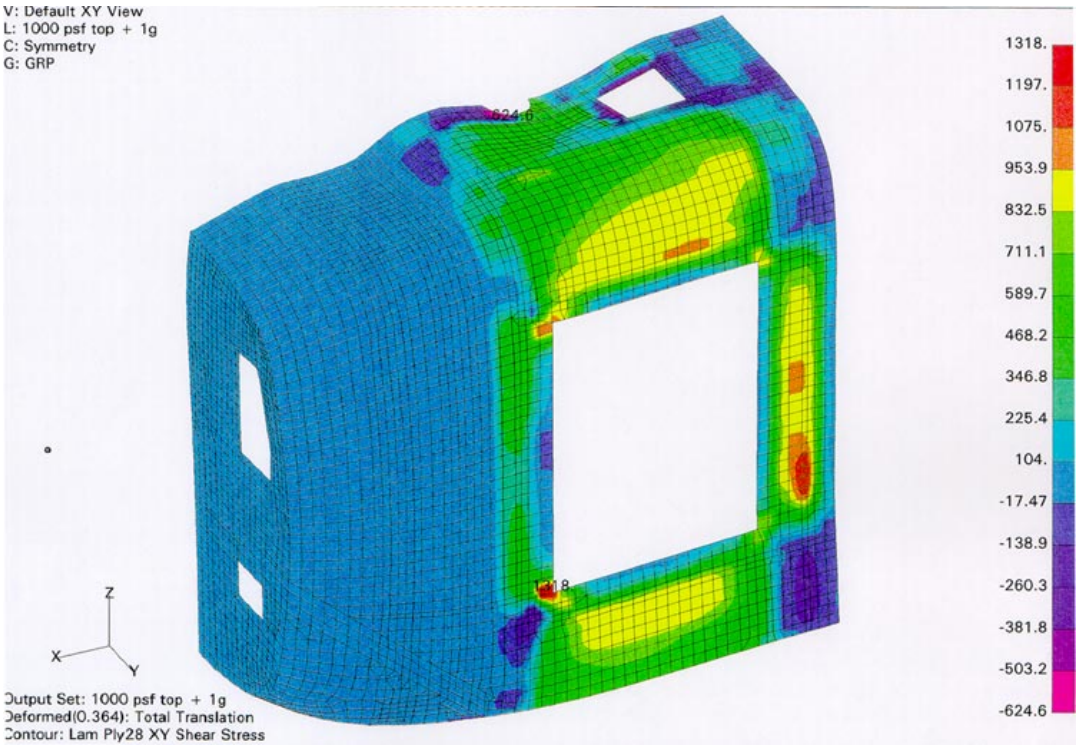

Figure 6: Shell Shear Stress For 1000 PSF Case

Figure 7 shows a typical fill stress distribution in the carbon channels.

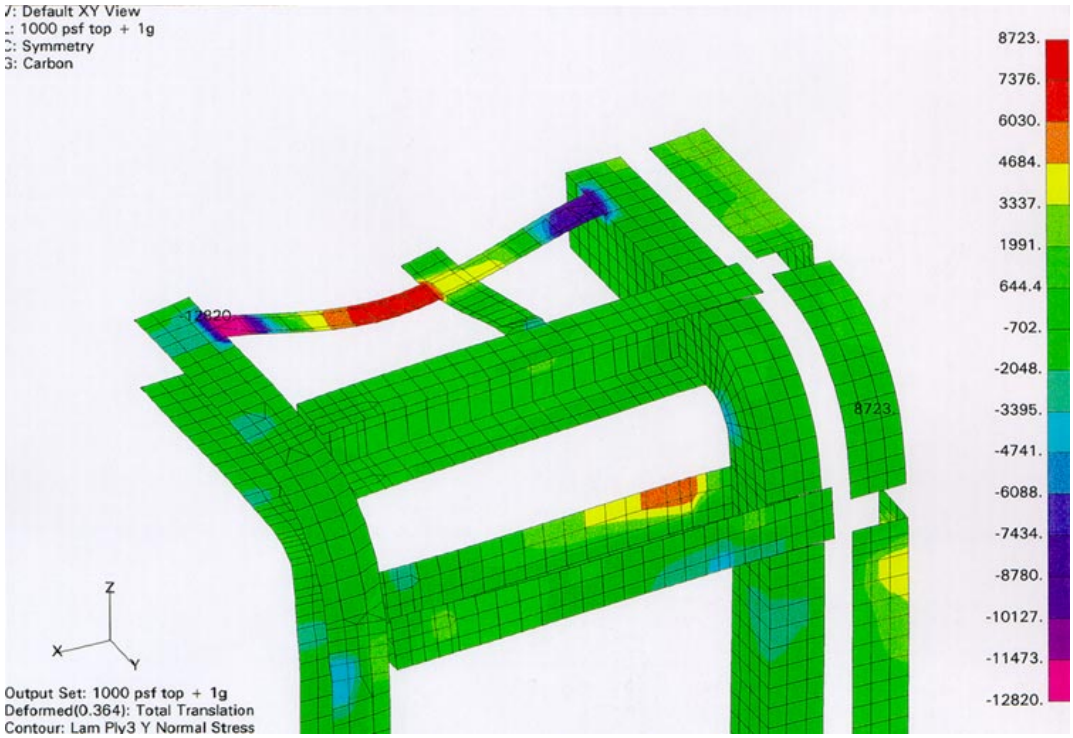

Figure 7: Fill Stress In Carbon Channels For 1000 PSF Case

Figure 8 shows a typical shear stress distribution in the VARTM glass bulkhead.

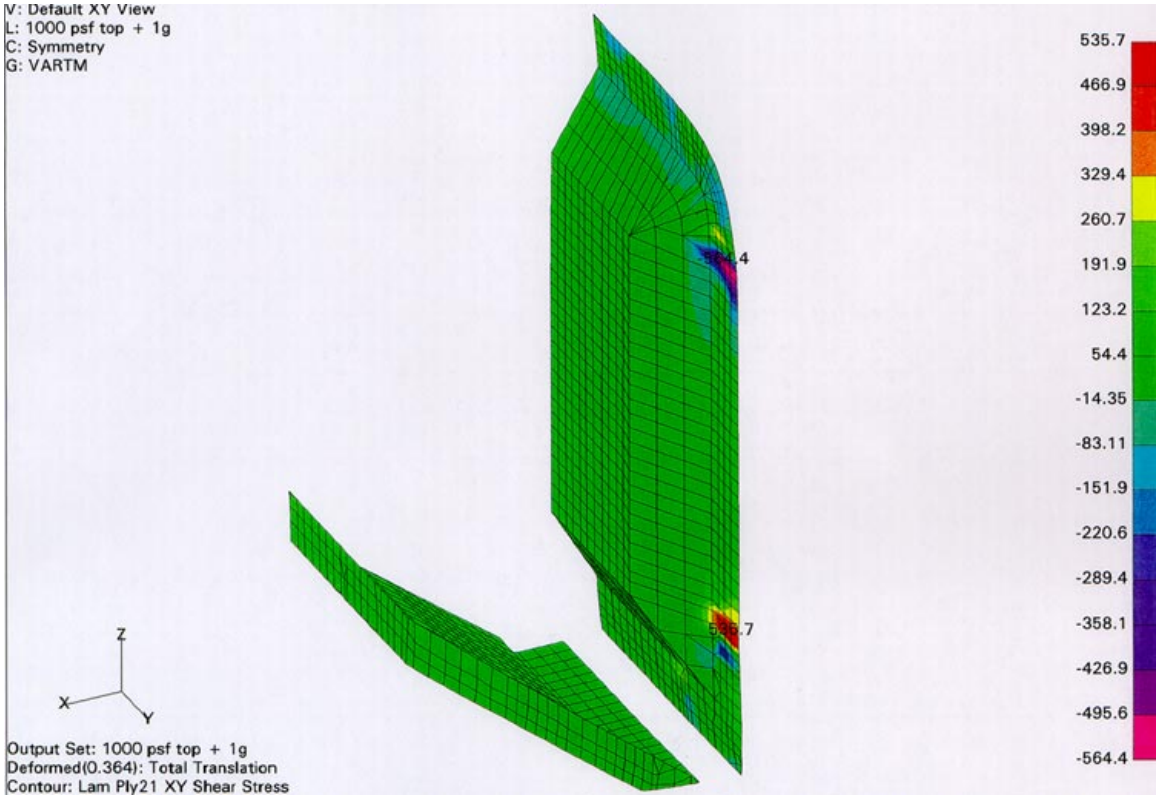

Figure 8: Shear Stress In VARTM Bulkhead For 1000 PSF Ca

The above are representative results. The process of checking each lamina stress component would be a time consuming process if done manually. Instead, each material system was sorted for values above a threshold level using the FEMAP [2] pre/post-processing software.

6] Clevis Analysis

The most critical connection is the attachment of the fairing structures to the pressure hull. Lugs are provided on the hull structure to attach the nose/aft fairing structures. A detailed analysis of the connection to these lugs was performed to assess the integrity of this joint. The nose/aft fairings have titanium fittings with a clevis feature to attach to the lugs. Each clevis slips over a mating HY-80 lug welded to the submersible support collar; an MP35N (nickel-cobalt based multiphase alloy) pin inserted through the clevis/lug fitting completes the connection. As these are the only connection points between the submersible Nose and Aftbody Fairings and the submersible support collar, a series of detailed solid finite element models were created to analyze

the stress/strain levels present in the clevi under “worst case” design load conditions.

In order to determine the clevis strain levels, elastic-plastic analyses were performed using the finite element code MSC/NASTRAN. Elastic-plastic static analyses were performed on detailed finite element (FE) models of selected clevi and surrounding fairing structure. Selection of clevi to be analyzed and model loads were based upon the results of previous analyses performed for the submersible Nose and Aftbody.

Figure 9 is a finite element representation of a “generic” clevis, showing the general characteristics of the clevis.

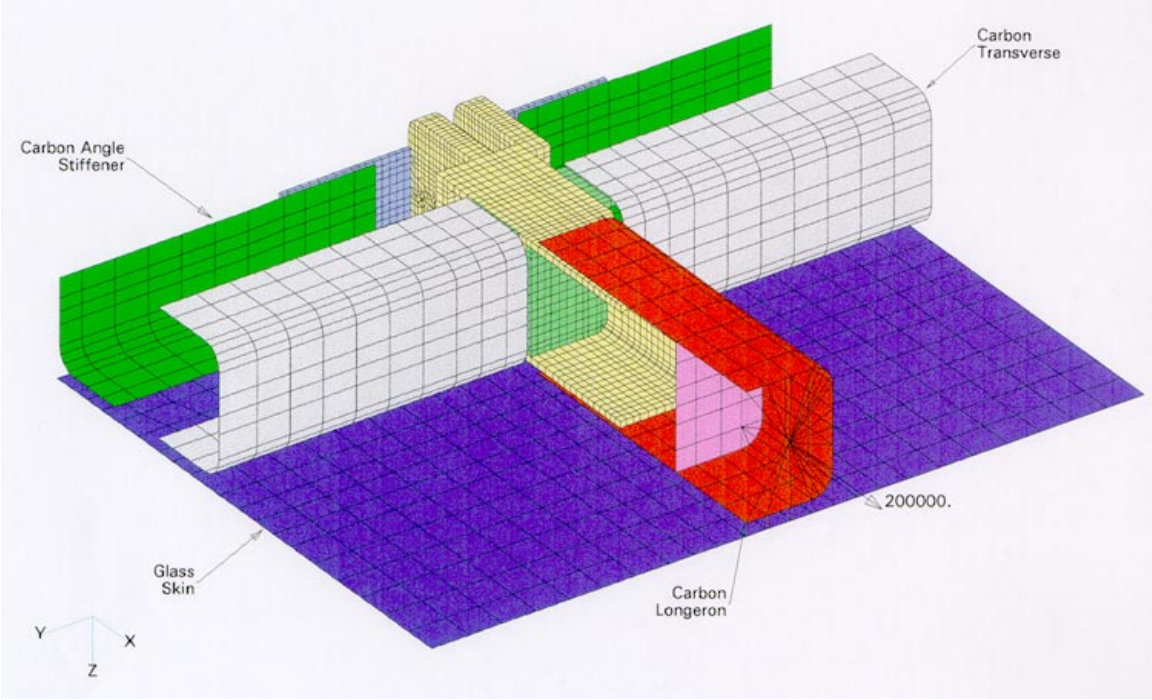

Figure 9: NASTRAN Model Of “Generic” Clevis

In general, the clevis is composed of a center core of machined Ti-6AL-4V titanium, approximately 21 inches long. One end of this center core is machined to fit over a mating HY-80 steel support collar lug; the opposite end is shaped and machined to fit snugly inside of a Fairing carbon longeron. Bolting surfaces for connecting the clevis to carbon transverses and carbon angle stiffener are provided by welding Ti-6AL-4V “tabs” to the sides of the center core.

Each clevis is bolted to the carbon beams which comprise the interior framework of the Fairing structure, using a pattern of 1/2” diameter MP35N bolts. Each clevis is then connected to the support collar of the submersible

pressure hull by an MP35N pin that joins the clevis to its mating HY-80 steel lug. Lateral constraint of the Fairing structure is provided by MP35N jack screws on the clevis, which bear down upon either side of the support collar lug.

As mentioned earlier, the submersible has a total of sixteen clevi (eight forward and eight aft). While the general configuration of each clevis is the same, there are specific differences in the particular geometry of each. These differences are due to the varying geometries of the particular carbon beams into which each clevis fits. These beams have varying degrees of curvature and twist, depending upon their location in the fairing structure. For example, the transverse tabs on the clevi on the sides of the fairing structures are relatively flat; the tabs on one side of the top clevis, on the other hand, have a degree of curvature due to the curvature of the carbon beams in the corner of the fairing structure.

The generic clevis model is exactly what its name implies - a generic representation of a “typical” clevis. As discussed earlier, there is no single geometry which is completely accurate for each submersible clevis. Each has a unique geometry, based upon its location on the Support Collar, the geometry of the carbon beams which are attached to it, and other factors. The generic clevis is an idealized version of all 16 clevi, with all bend and twist taken out of its various components. Since there is no twist or bend in this model geometry, it was significantly easier to construct than the models representing actual clevis and fairing geometries. As such, it was used to obtain an initial “quick look” at the strain levels in the clevis under loading. This model was loaded by applying a longitudinal force of 200,000 lb. to the end of the carbon longeron; this is meant to represent the worst load case, which produces a maximum longitudinal reaction of 197,697 lb. (201,253 lb. total shear reaction) at the top clevis/lug joint.

The second model constructed for this analysis was the “Aftbody top clevis model”. This model was constructed by “cutting out” the portion of Fairing structure around the top clevis in the global Aftbody symmetry model. The portion of the Aftbody structure cut out of the global model is shown in Figure 10.

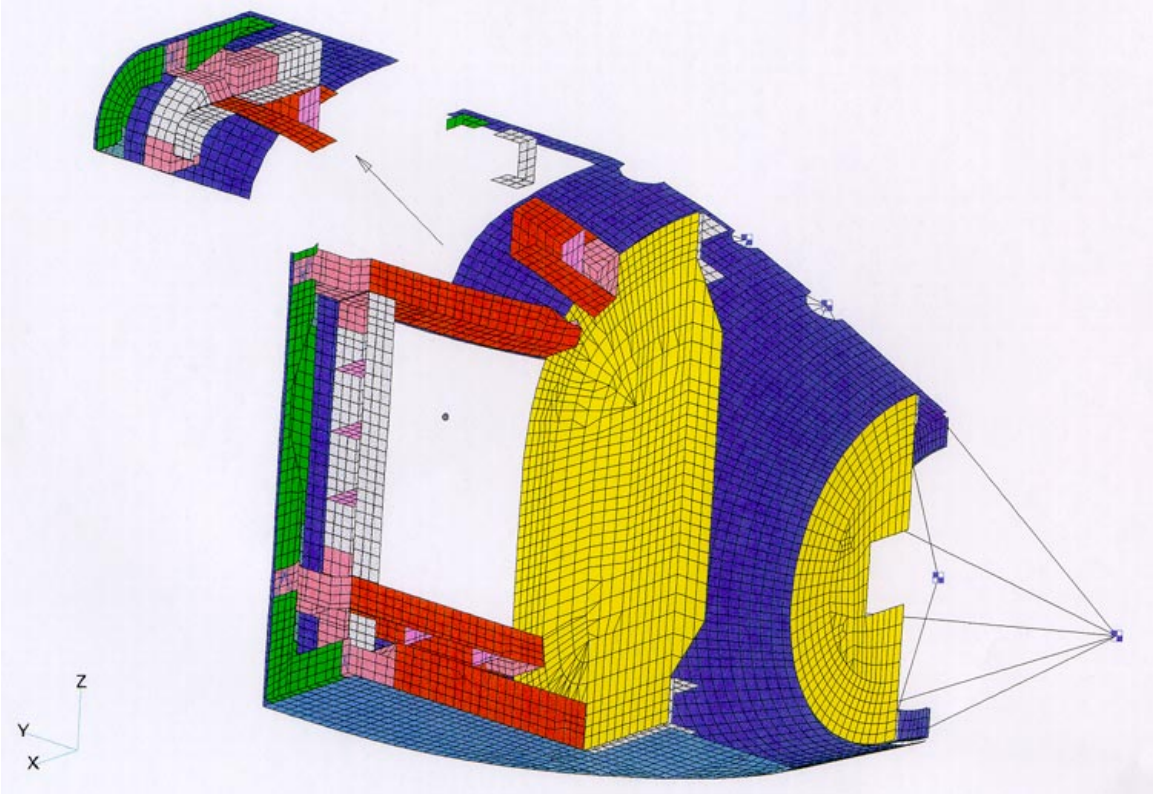

Figure 10: Local Cutout For Aft-Body Analysis

A detailed solid model of the clevis was then built into this section of the global model. The model was loaded by applying enforced displacements at the nodes along the "cut edges" of the laminate structure (skin and beams). The enforced displacements used in the analysis were taken from the results of the worst case loading analysis performed on the global model. This is the load case which produced the maximum lug/clevis joint reaction. The Aftbody top clevis model is shown in Figures 11 and 12.

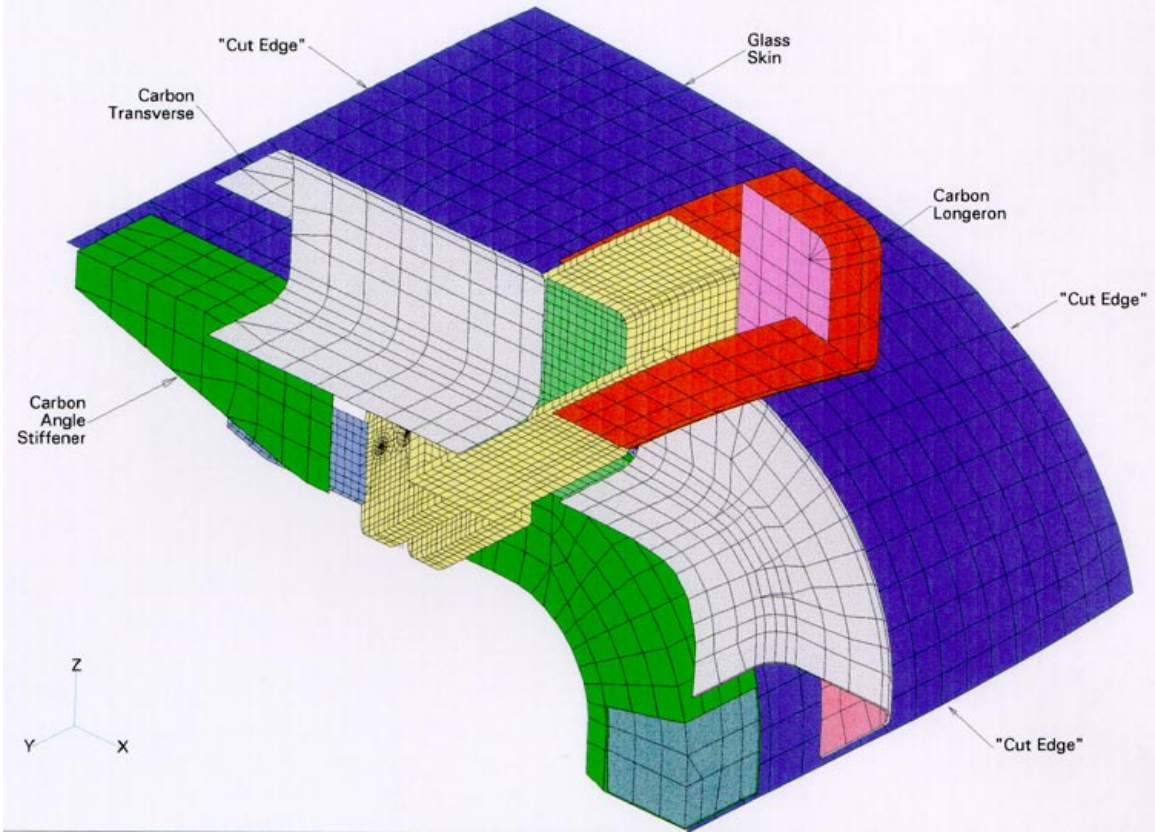

Figure 11: Aft-Body Clevis Analysis Model

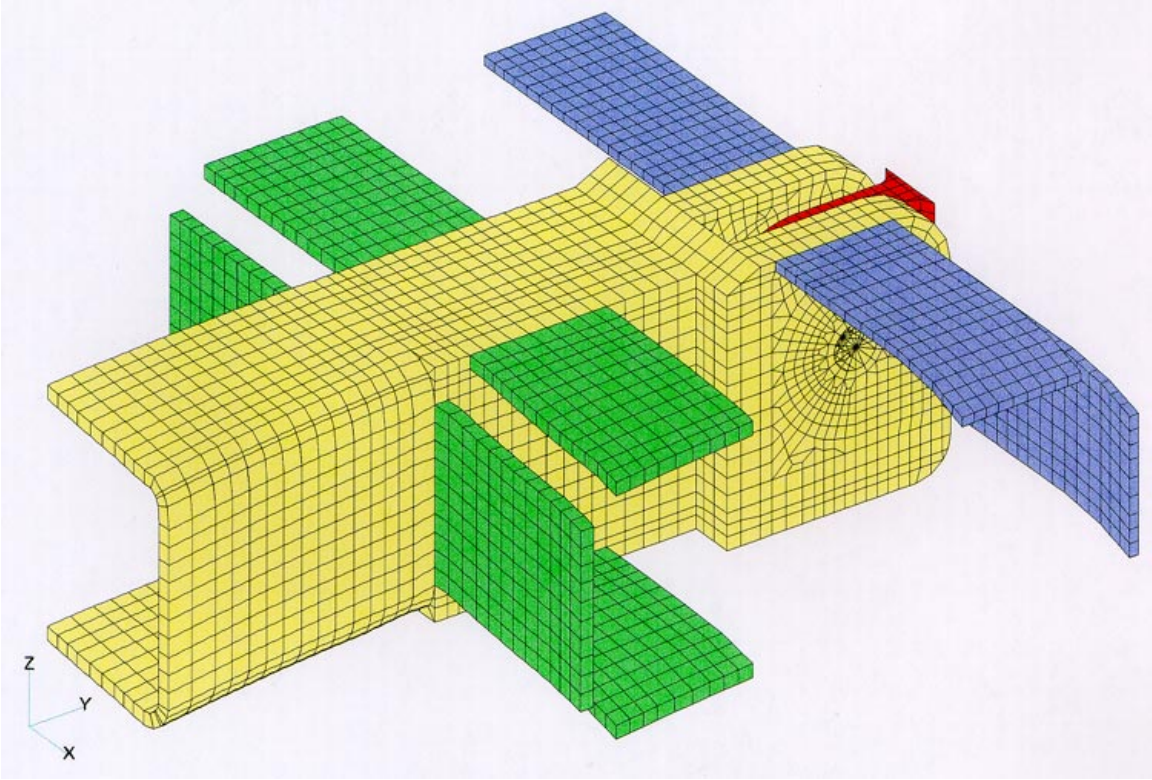

Figure 12: Metallic Components In Aft-Body Clevis Model

All composite lamina in the submersible clevis models are modeled using layered shell elements as described above. These include the E-Glass outer skin and floor, and the carbon angle stiffener, longerons, and transverse beams. Individual ply thicknesses, material sets, and angular orientations for each particular lamina are fully detailed in the element descriptions. The titanium clevis and HY-80 steel Lug are modeled using 8-noded solid elements (CHEXA elements). All bolts, screws, and pins are modeled using bar elements (CBARs), and connectivity between the clevis and the MP35N main pin and jack screw is accomplished using stiff rods (CRODs).

To begin the detailed analysis of this clevis, a portion of the Aftbody global FE model is isolated and removed. The crude representation of the lug/clevis joint used in the global model is then replaced with detailed solid representations of the titanium clevis and the HY-80 steel lug. This becomes the baseline clevis FE model.

The MP35N main pin is modeled using bar elements along the pin axis; these bar elements have the inertial properties of the 1.18” diameter pin. The pin axis is connected to the titanium clevis and the HY-80 steel lug using a series of stiff rods in a “wagon wheel” pattern, as shown in Figure 13. The MP35N jack screw is modeled in a similar manner.

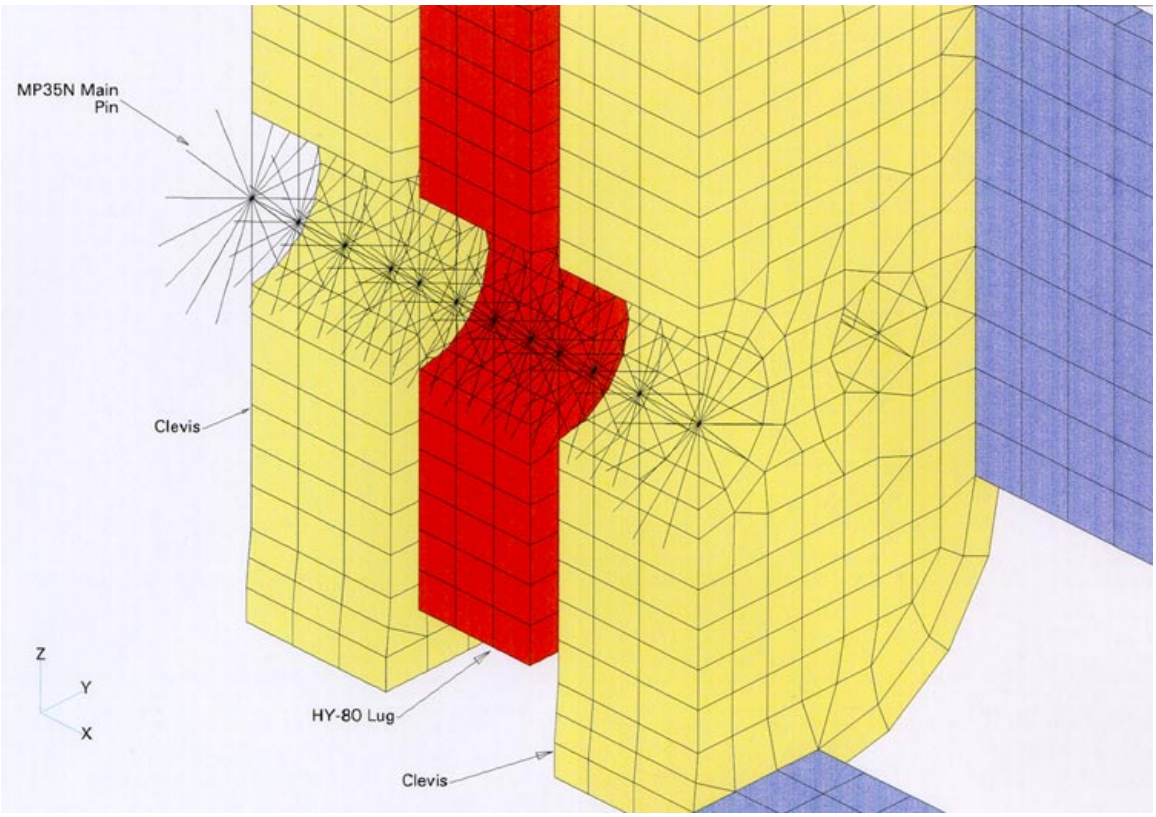

Figure 13: Pin Load Transfer Model

The model is loaded by imposing enforced displacements at the nodes along the "cut edges" of the skin, floor, and carbon beam. In this illustrative example, the enforced displacements are the nodal displacements taken from the Aftbody global analysis. In the global analyses of the Aftbody and Nose Fairings, SDOF (single degree of freedom) springs were used to model the compliance of the support collar at each lug. Similarly, SDOF spring are applied to the base of the HY-80 steel support collar lug in the detailed model.

The first step in the analysis process is to compare the overall behavior of the detailed clevis model with the behavior of the global analysis model. To do this, a linear static analysis of the detailed clevis model is performed using the enforced displacements taken from the global model. After the first run is complete, the loads in the rods which make up the "spokes" in the main pin and jack screw "wagon wheels" are examined to determine whether the members are in tension or compression. Physically, any tension members provide unrealistic load paths, as they "pull" on the edges of the clevis or lug holes. Any members in tension are modified so that their stiffness is effectively set to zero, and the analysis is repeated. This process is continued in an iterative manner until no "spokes" are in tension.

Once all the tension members have been removed from the model, the total force reactions at the lug are determined and compared to the reactions obtained from the global analysis model. If there is a significant difference in the reactions, then the stiffnesses of the SDOF springs at the base of the lug are adjusted and the analysis is repeated. Again, the analysis is repeated in an iterative manner until the force reactions obtained from the detailed clevis model closely match the force reactions obtained from the global model. This provides a level of confidence that the detailed model and the global model are behaving in a similar manner, and are representative of the same load levels. The rods comprising the Main pin and jack screw spokes are again checked to make sure that no members have gone into tension as the spring stiffnesses have been modified. Table 2 is a comparison of the force reactions at the Aftbody bottom clevis, for the global and detailed models.

Table 2. Comparison of Global Model and Detailed Model Lug Reactions

	Aftbody Global Model	Detailed Clevis Model	Percentage, Detailed/Global
Longitudinal Reaction (lbs)	-77,927	-76,697	98 %
Athwartship Reaction (lbs)	65,710	55,218	84 %
Vertical Reaction (lbs)	-11,644	-7,187	62%

The good agreement between the global and detailed models in the major component reactions (longitudinal and athwartship directions) shows the detailed model adequately represent the behavior of the global model.

As an additional check that the global and detailed models are behaving similarly, the laminate stresses in the skin for both models are compared. Again, confidence in the detailed model is gained by matching the global model analysis results. Stress agreement was within 10% from the two analyses.

Once the linear static analysis has established that the detailed model behaves in a similar manner to the global model, then an elastic-plastic static analysis of the detailed model is performed to determine the plastic strains in the clevis. Elastic-plastic material stress-strain curves are input for titanium and MP35N, and an elastic-plastic static analysis is performed.

7] Clevis Results

The Aftbody top clevis model was shown in Figures 11 and 12. This model was constructed by “cutting out” the portion of Fairing structure around the top

clevis in the global Aftbody symmetry model as previously described. The model was loaded by applying enforced displacements at the nodes along the "cut edges" of the laminate structure (skin and beams). The enforced displacements used in the detailed analysis were taken from the results of the worst case analysis performed on the global model. This is the load case which produced the maximum lug/clevis joint reaction (201,253 lbs).

A static linear analysis was first performed to identify and eliminate tension rods in the pin and jack screw representations, and to "tune" the spring stiffnesses representing the support collar compliance. The force reactions at the HY-80 steel lug were then compared to the reactions from the Aftbody global analysis. Table 3 is a comparison of the force reactions at the Aftbody top clevis under the worst case loading, for the global and detailed models.

Table 3. Comparison of Global Model and Detailed Model Lug Reactions

	Aftbody Global Model	Detailed Clevis Model	Percentage, Detailed/Global
Longitudinal Reaction (lbs)	196,697	186,800	94 %
Athwartship Reaction (lbs)	-13,847	-13,595	98 %
Vertical Reaction (lbs)	37,670	30,291	80 %

As an additional check that the global and detailed models were behaving similarly, the laminate stresses in the skin for both models were compared. Table 4 is a comparison of typical ply stresses in the skin around the Aftbody top clevis (global model) and the detailed Aftbody top clevis model.

Table 4. Comparison of Global Model and Detailed Model Ply Stresses

	Aftbody Global Model	Detailed Clevis Model	Percentage, Detailed/Global
Ply 1 X-Normal Stress (psi)	9,737	9,304	96 %
Ply 1 Y-Normal Stress (psi)	-12,488	-13,210	106 %
Ply 1 XY Shear Stress (psi)	4,731	4,805	102 %
Ply 2 X-Normal Stress (psi)	-12,132	-10,937	90 %
Ply 2 Y-Normal Stress (psi)	11,581	11,446	99 %
Ply 2 XY Shear Stress (psi)	-3,834	-3,836	100 %

After performing the linear static analysis to identify and eliminate tension members in the main pin and jack screw components, an elastic-plastic static analysis was performed. Figures 14 through 16 show the results of this analysis. The maximum plastic strain in the clevis is found to be 0.83 % which is well below the ultimate for this material, and occurs in a localized area at the "back" of the main pin hole.

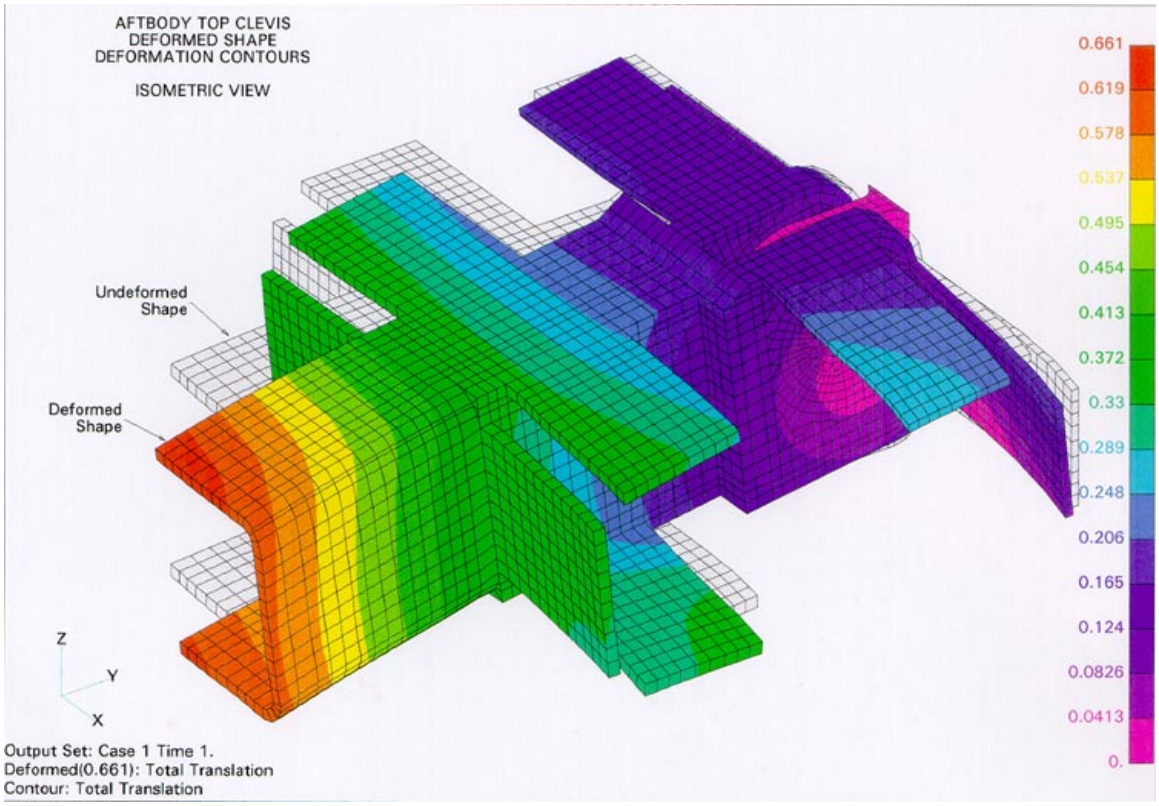

Figure 14: Aft-Body Clevis Deformed Geometry

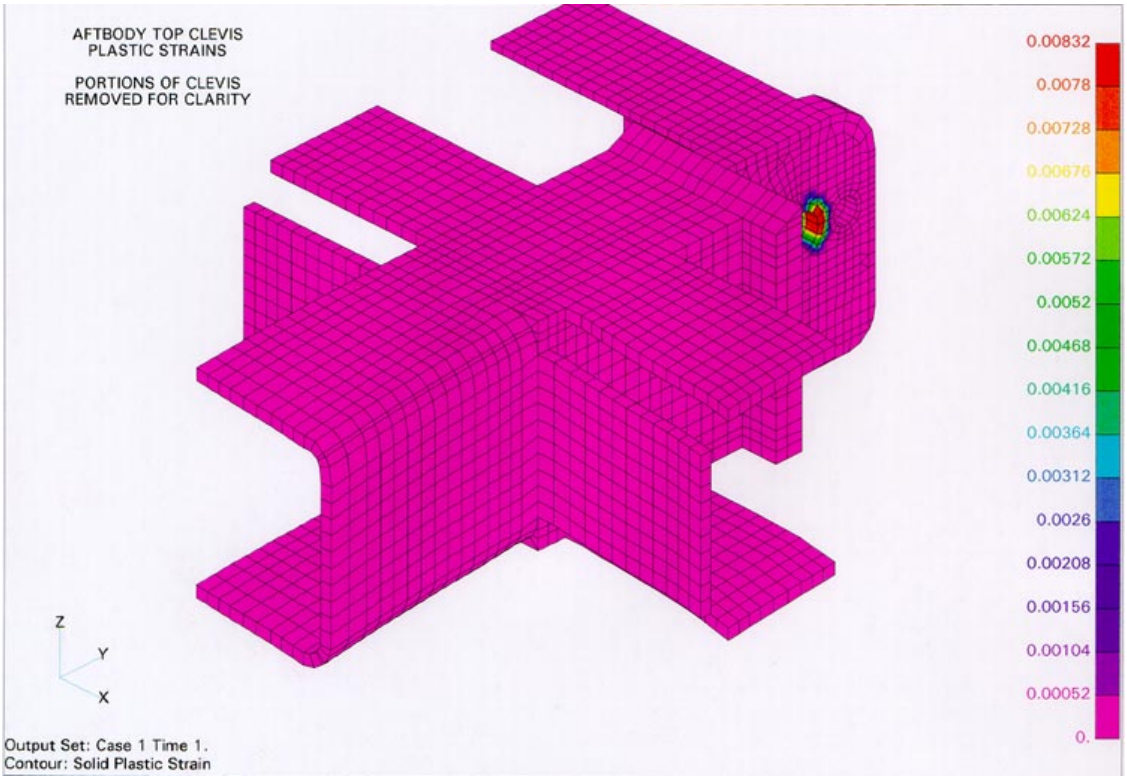

Figure 15: Aft-Body Clevis Plastic Strains

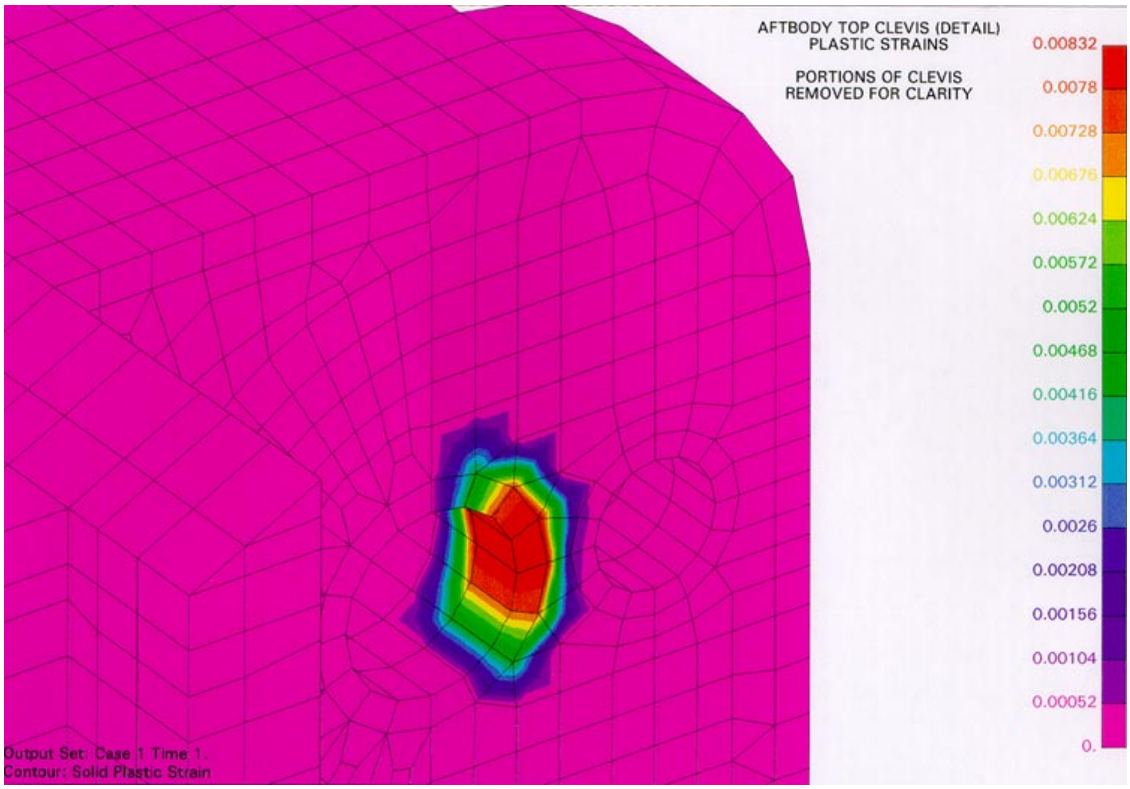

Figure 16: Detailed Distribution Of Plastic Strains

8] Conclusions

This paper summarizes some of our efforts using MSC NASTRAN as the analysis tool for the design of composite fairings for a submersible. For the laminated composites, the formulation in MSC NASTRAN provides accurate lamina stress predictions (linear elastic behavior assumed) as previously validated by comparison with test data. Modeling approaches to bolted connections, bolt bearing concerns and joint load transfer issues exist and allow the user significant flexibility. For linear static analyses, the code performed very efficiently and allowed for dynamic design studies in a timely manner.

The clevis analysis allowed us to explore the use of MSC NASTRAN for elastic-plastic problems. While limited to a small strain formulation, it is believed that the answers obtained are sufficient for design assessment. Indeed, in another aspect of the program, we performed elastic-plastic analysis for an HY-80 steel component which exhibited large plastic strains. The problem was analyzed using MSC NASTRAN (small strain assumptions) and ANSYS (large strain assumptions). Agreement was demonstrated between the two codes to approximately 10% plastic strain (for that application).

9] References

1] MSC NASTRAN is available from: the MacNeal-Schwendler Corporation, 815 Colorado Blvd., Los Angeles, CA 90041. Version 69 was used in this work.

2] FEMAP is available from: Enterprise Software Products, P.O. Box 1172, Exton, PA 19341. Version 4.5 was used in this work.